Bulk phonon scattering in perturbed quasi-3D multichannel crystallographic waveguide



2008 J. Phys.: Condens. Matter 20 465218

(http://iopscience.iop.org/0953-8984/20/46/465218)

J. Phys.: Condens. Matter **20** (2008) 465218 (11pp) doi:10.1088/0953-8984/20/46/465218

# Bulk phonon scattering in perturbed quasi-3D multichannel crystallographic waveguide

**M S Rabia**

Laboratoire de Mécanique des Structures et Energétique, Département de Génie Mécanique, Faculté du Génie de la Construction, Université M. Mammeri, Tizi-Ouzou 15000, Algeria

E-mail: m2msr@yahoo.fr

Received 16 March 2008, in final form 15 September 2008
Published 27 October 2008
Online at stacks.iop.org/JPhysCM/20/465218

**Abstract**

In the present paper, we concentrate on the influence of local defects on scattering properties of elastic waves in perturbed crystalline quasi-three-dimensional nanostructures in the harmonic approximation. Our model consists of three infinite atomic planes, assimilated into a perfect waveguide in which different distributions of scatterers (or defects) are inserted in the bulk. We have investigated phonon transmission and conductance for three bulk defect configurations. The numerical treatment of the problem, based on the Landauer approach, resorts to the matching method initially employed for the study of surface localized phonons and resonances. We present a detailed study of the defect-induced fluctuations in the transmission spectra. These fluctuations can be related to Fano resonances and Fabry–Pérot oscillations. The first is due to the coupling between localized defect states and the perfect waveguide propagating modes whereas the latter results from the interference between incidental and reflected waves. Numerical results reveal the intimate relation between transmission spectra and localized impurity states and provide a basis for the understanding of conductance spectroscopy experiments in disordered mesoscopic systems.

(Some figures in this article are in colour only in the electronic version)

## 1. Introduction

Scattering and localization phenomena in disordered mesoscopic systems have been well established both experimentally [1] and theoretically [2]. They are actually of renewed interest owing to advances in nanotechnologies, the basic motivation being to understand the limitations that structural disorder may have on physical and mechanical properties of crystalline materials. Our present knowledge of the related phenomena has been given by the work of Landauer [3], in which the sample studied is represented by a series of scatterers (or defects) inserted in the bulk or on the surface of a perfect waveguide, made it possible to connect the conductance of the sample to its scattering matrix. His interpretation has stimulated many researchers [4–8] to look for the effects of quantum coherence in dc transport in particular. Recently, several authors [9–14] have shown that multiple scattering and quantum interference become very important in describing transport phenomena, localization of electron states in disordered media [1, 3, 6], coherent magnetotransport [1, 7] and to investigate structural properties of low-dimensional samples [6, 9, 10].

In the present work, we concentrate on the influence of localized impurities on scattering properties of vibrational waves in perturbed quasi-three-dimensional crystalline structures in the harmonic approximation [12]. While there has been interest in electronic phenomena for many years, the study of vibrational waves by completely *ab initio* techniques is still a difficult task. The numerical treatment of the problem, based on the Landauer principle, resorts to the matching method [15, 16] initially employed for the study of surface localized phonons and resonances. This method already gave satisfactory results for electronic phenomena [4, 5] and wave scattering [8–12].

In the following, we shall show that the different nature of vibrational waves gives rise to some interesting properties.

 

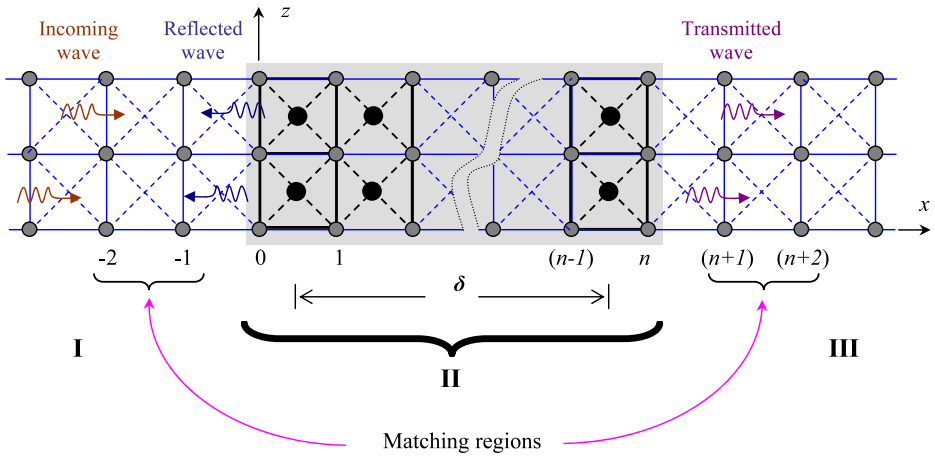


**Figure 1.** Two-dimensional cross section of perturbed crystallographic waveguide modelled by a triple infinite atomic plane. The shaded area II indicates the defect region, while areas I and III are two semi-infinite perfect waveguides. The perturbed region contains defect masses and defect springs.

As in the electron case, we find that the conductance spectra of vibrational waves can be regarded as identifying characteristics of the structural properties of the considered system. Multiple scattering causes a large variety of resonance features identified as Fano resonances, due to a coupling between continuum propagating modes and defect-induced states and Fabry–Pérot oscillations resulting from the interferences between incidental and reflected waves in the perturbed area.

The complexity in the present vibrational study is enhanced, as compared to previous work concerning quasi-one-dimensional waveguides, by the need to treat the increased dimensionality of the considered system.

The organization of this paper is as follows. After a brief summary description of the method employed, section 2 is interested in the dynamical properties of the perfect waveguide and the presentation of the algebraic formalism for scattering in the presence of defects. Section 3 will be devoted to the calculation of the transmission coefficient and its evolution in terms of the defect mass and of the bonding constants in the perturbed region.

## 2. Principle of the method

The matching method, initiated by Feuchtwang in 1967 and developed by Szeftel *et al* in 1987 [16], accounts in a satisfactory way for the phonon dispersion curves [6] and surface resonances. It also gives a more general definition of the concept of resonance and allows a more transparent analysis of the displacement behaviour in the vicinity of Van Hove singularities [17]. Its implementation requires the crystal's subdivision into three distinct regions, all having the same two-dimensional periodicity along the surface (figure 1):

(i) A bulk region having three-dimensional (3D) periodicity representing the crystal without defect (perfect waveguide) where the dispersion curve is first worked out. It is assimilated into regions I and III of figure 1.

(ii) A perturbed region consisting of an arbitrary number of adsorbate, reconstructed or relaxed layers, inside which the translational symmetry is lost along that direction not contained in the surface plane. It is represented by region II of figure 1.

(iii) An intermediate region of bulk matter, the thickness of which increases with increasing range of inter-layer interactions, used to match bulk phonons with the boundary conditions imposed by the surface, from which the technique was given the name 'matching method'. In our case, this area is represented on both sides of region II by the matching areas which make it possible to relate the defect atomic displacements to those of the two semi-infinite waveguides I and III (figure 1).

### 2.1. Dynamics of the perfect lattice

The geometry of the structure studied sketched in figure 1 is modelled by three lattice planes always parallel to the $x$–$y$ plane. It consists in a 3D simple cubic lattice with nearest- and next-nearest-neighbour interactions. This approximation seems reasonable in the condensed matter context [8]. In the I and III unperturbed regions, elastic constants between first neighbours are indicated by $k_1$ and those between second ones by $k_3$. The other force constants are indicated by different features on the diagram from figure 1. The perturbed region II itself (grey area in the figure), composed of isolated scatterers or interstitial defects positioned in the centre of the $xz$ face of the cubic crystal, extends over columns 0 to $n$. Defect planes are separated by a distance $\delta$. For simplification reasons, the edge length $a$ of the cube is taken equal to unity.

The matching method that we employ has previously been extended to study wave scattering in quasi-1D disordered mesoscopic systems [8, 9, 11]. The equation of motion of an atom $(l)$ at the frequency $\omega$ is given as usual in the harmonic approximation [12] by

$$\omega^2 m(l) u_\alpha(l,\omega^2) = -\sum_{l' \neq l} \sum_{\beta} K(l,l') \frac{r_\alpha r_\beta}{d^2} \times [u_\beta(l,\omega^2) - u_\beta(l',\omega^2)], \quad (1)$$

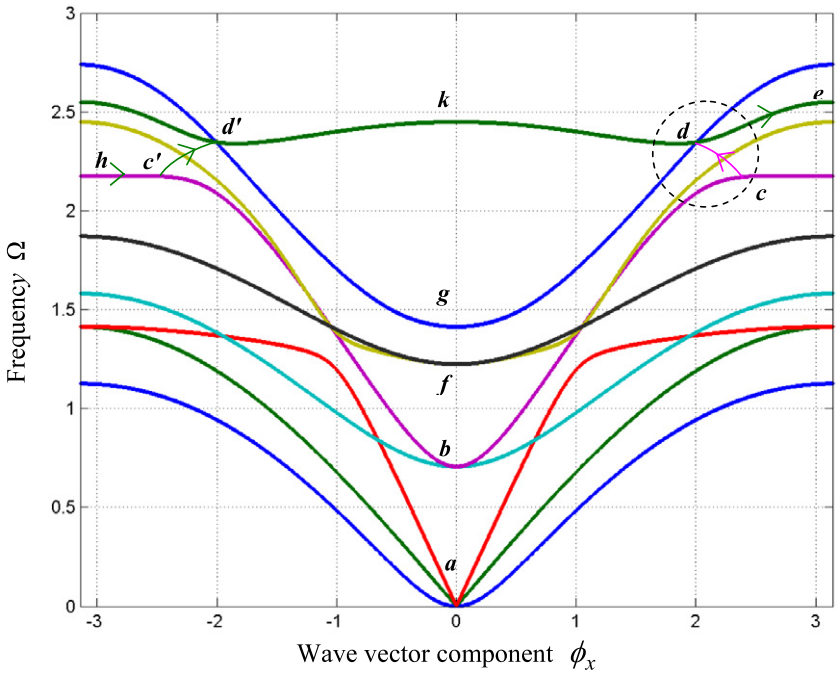


**Figure 2.** Dispersion branches for the bulk phonon propagating modes of the triple plane with $\phi_x$ running over the first Brillouin zone $[-\pi/a \quad \pi/a]$, for the case of a null incidence angle.

where $\alpha, \beta \in \{x, y, z\}$ indicate the different Cartesian directions of space. $m = m(l)$ is the atomic mass located at the site $(l)$, $u_\alpha(l, \omega^2)$ is the displacement field along the $\alpha$ direction; $r_\alpha$ is the corresponding Cartesian component of the relative radius vector between sites $(l)$ and $(l')$, and $d$ represents the distance $ll'$, whereas $K(l, l')$ is the bonding strength constant between the atoms occupying these sites. Let us recall that the summation concerns all the first and second neighbours of the site $(l)$. Moreover, to take account of the modification of the strain field in the perturbed region, we will define a parameter $\lambda$ indicating the relationship between the modified force constants (region II) and those of the perfect areas I (left) and III (right-hand side), see figure 1.

In the $Ox$ propagating direction, the elastic wave can be attenuated when meeting the defect. It would be convenient, in this case, to introduce a phase factor $Z$ (not to be confused with the $z$ direction) relating displacements of two adjacent atomic sites:

$$u_x(n \pm 1, p) = Z^{\pm 1} u_x(n, p). \tag{2}$$

The attenuated wave is described by a value of $Z$ whose modulus is lower than unity, whereas the propagating wave is given by $z = e^{iq_x a} = e^{i\phi_x}$, where $q_x$ is the component along the $Ox$ axis of the reciprocal lattice wavevector $\vec{q}$. This phase relation is an essential feature of the matching method [15, 16], initially employed for the calculation of surface phonons and resonances. Note that in the $Oy$ direction, parallel to the perturbating atomic chain, $Z$ is defined by $e^{iq_y a_y} = e^{i\phi_y}$ in accordance with the Bloch function. Vibrational displacements along the $Oy$ axis are bound by the equality

$$u_y(n, p \pm 1) = e^{\pm i\phi_y} u_y(n, p). \tag{3}$$

Taking into account the relations (2) and (3), the perfect lattice atom equation of motion (1) rewrites itself in the following matrix system:

$$[\Omega^2 I - D(\phi_y, r_3, Z)]|u\rangle = |0\rangle, \tag{4}$$

where $\Omega^2 = m\omega^2/K(l, l')$ is the dimensionless frequency, $I$ is the identity matrix, $D(\phi_y, r_3, Z)$ is the perfect lattice dynamical matrix (regions I and III) and $|u\rangle$ is the vector displacement. $r_3$ denotes the force constant ratio between nearest and next-nearest neighbours.

For fixed $r_3 = k_3/k_1 = 0.5$ and $Z = e^{i\varphi_x}$, the resolution of equation (4) determines the eigenfrequencies of vibration $\Omega_\nu$ as well as the corresponding eigenvectors $\vec{u}_\nu$. The nine propagating modes of the triple plane correspond to the solution $Z = 1$. When $\phi_x$ is running over the first Brillouin zone $[-\pi/a \; \pi/a]$, one obtains the dispersion curves $\Omega(\phi_x)$. Figure 2 shows the shape of these curves, symmetrical relative to the frequency axis, for a null incidence angle. Contrary to the electronic case where the curves are parallel sinusoids, we do not have here any hope of finding a usable analytical expression. It will thus be necessary to resort to purely numerical methods to integrate these dispersion relations in the general problem in the presence of a defect.

For a null incidence angle, the three first modes are acoustic and the six others are optical. All modes become optical for any other value of $\phi_y$. Moreover, the dispersion branches overlap at a certain frequency interval which decreases when $\phi_y$ increases. So we must expect that the modes will be simultaneously excited in these regions. The examination of eigenvectors shows that modes 3, 5 and 8 (classification being done upwards) are polarized longitudinally whereas the rest of the modes are polarized

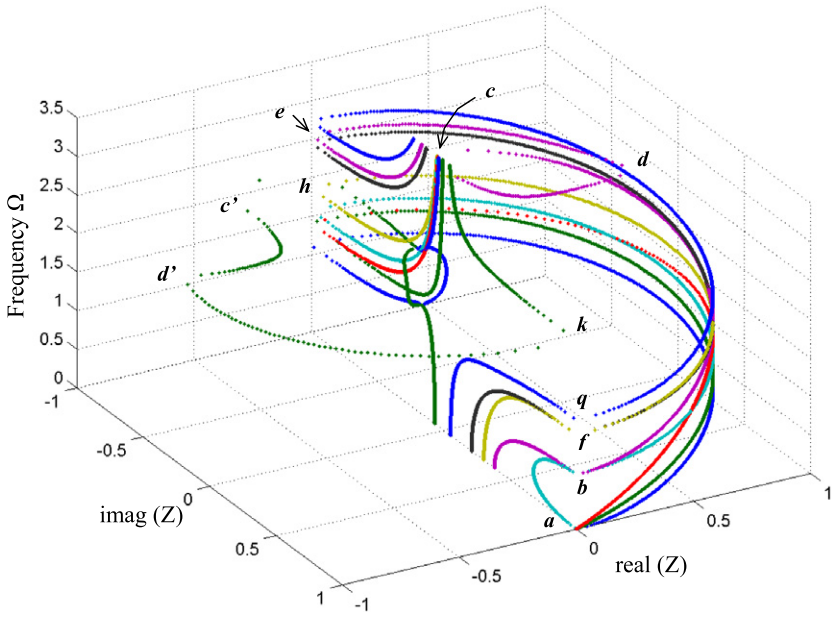


**Figure 3.** Functional behaviours $\Omega(Z)$ of the vibrational modes characterizing the triple atomic plane. Unit circles correspond to propagating modes (dispersion curves $\Omega(\phi_x)$ of figure 2) whereas the evanescent modes are represented by the parts inside the unit circles.

transversely. These polarizations are typical for other values of $\phi_y$. Note that the lowest acoustic branch appears to exhibit a nonlinear variation in the long-wavelength limit [18]. This behaviour is a consequence of the finite extension of the waveguide in the $z$ direction.

In addition to the propagating modes described previously, the scattering in the presence of a defect also requires the determination of the evanescent modes ($|Z| < 1$) of the system. Although the evanescent modes do not contribute to energy transport they are necessary for a full description of the scattering problem. These solutions can be obtained by different procedures [10]. An elegant and well-suited way used in similar electronic problems [7, 19] consists of increasing the space eigenvectors basis by introducing new unknowns defined by

$$\vec{v}_\beta(l) = -\frac{1}{Z}\vec{u}_\alpha(l). \tag{5}$$

We then rewrite equation (2) in the form of an eigenvalue problem for $Z$:

$$A(\omega, r_3, \phi_y)\vec{W} = ZB(r_3, \phi_y)\vec{W} \qquad \text{with } \vec{W} = \begin{pmatrix} u_\alpha(l) \\ v_\beta(l) \end{pmatrix}, \tag{6}$$

where the $A$ and $B$ matrices, of dimension $(18 \times 18)$, come from the basis change. Note that the dimension of this generalized eigenvalue problem is twice as large as the original problem.

The solution of equation (6) yields nine pairs of eigenvalues $Z$ and $Z^{-1}$, which must be sorted. As discussed above, eigenvalues with $|Z| = 1$ correspond to propagating waves, which are described by real wave vectors. These solutions can be grouped in pairs corresponding to the two directions of propagation. Both solutions are linked by time-reversal symmetry. Owing to the fact that they contain the same information, we arbitrarily choose those which are propagated from the left to the right. Solutions with $|Z| \neq 1$ correspond to evanescent or divergent waves. Only the physically relevant evanescent modes are retained. Both propagating and evanescent solutions are needed for the description of the scattering in the presence of defects.

The functional behaviours $\Omega(Z)$ of the nine vibratory eigenmodes characterizing the triple plane are given in figure 3 for the case of an incidence angle $\phi_y = 0$. The projection of modes on the $Z$ complex plane shows that the propagating solutions $\Omega(\phi_x)$ of figure 2 are represented by the curves following the unit circles of radii equal to the phase factor modulus, whereas the evanescent solutions correspond to the curves contained inside the unit circles. In addition, the anticrossing phenomenon of the 5 and 9 optical modes, of the same symmetry, constrained phonons to take evanescent paths to jump from one propagating branch to the other in the interacting zone [10] (surrounded by a dotted circle in figure 2).

This spatial representation of the dispersion relations corresponds to the complex phononic band structure, real frequency versus complex phase factor $Z$, which presents a great similarity to the results obtained by Sainidou *et al* [20] using the layer-multiple-scattering method in the study of phononic crystals.

In order to show the correspondence between figures 2 and 3, we have marked common special points in both the $\Omega(Z)$ and $\Omega(\phi_x)$ representations. The paths followed by the phonons are also shown by arrows on the dispersion curves. It is then clear that the frequency ranges of propagating modes 3–9 will be slightly different, obviously, from that given by the dispersion curves of figure 2. Figure 4 shows the evolution of the attenuation factor as a function of the incident phonon frequency for each vibrating mode characterizing the waveguide. One can find that the plateau's length indicates

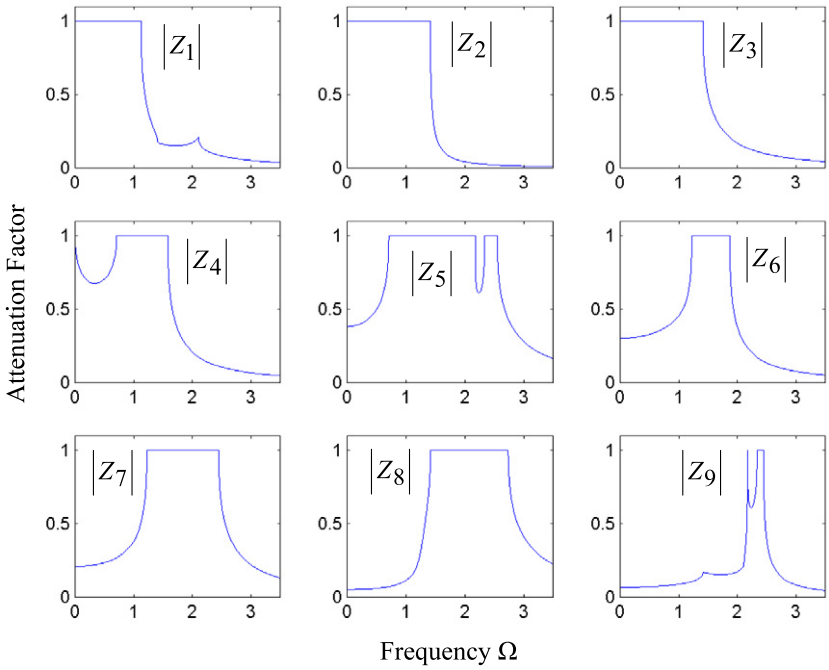


**Figure 4.** Attenuation factor evolution as a function of the dimensionless frequency for the waveguide eigenmodes. The extent of the plateau indicates the specific propagating frequencies range of each mode.

the new propagating frequency ranges of all nine waveguide modes.

### *2.2. Elastic scattering at defects*

The presence of defects in a waveguide modifies considerably the mechanical properties of the structure by creating new localized states and by diffusing phonons in the volume and on the surface. Since the perfect waveguides do not couple between different eigenmodes, we can treat the scattering problem for each eigenmode separately. For an incidental wave coming from the left to right (figure 1) in the eigenmode $\bar{\nu}$

$$\vec{V}_{\text{in}}^{\,i} = (Z_{\bar{\nu}})^i \vec{u}_{\bar{\nu}}, \tag{7}$$

where $Z_{\bar{\nu}}$ is the phase factor of the incoming wave, $\vec{u}_{\bar{\nu}}$ is its eigenvector; the exponent $i$ indicates the site occupied by the atom along the direction of propagation.

The resulting scattered waves, composed of a reflected and transmitted part, give rise to vibratory displacements $\vec{u}_r$ and $\vec{u}_t$ in the two half spaces $L$ and $R$, respectively. They can be expressed as a superposition of the perfect waveguide eigenmodes at the same frequency:

$$\vec{u}_r^{\,i} = \sum_{\nu} r_{\nu\bar{\nu}} \cdot \left[\frac{1}{Z_\nu}\right]^i \cdot \vec{u}_\nu\left(\frac{1}{Z_\nu}\right), \tag{8}$$

$$\vec{u}_t^{\,i} = \sum_{\nu} t_{\nu\bar{\nu}} \cdot [Z_\nu]^i \cdot \vec{u}_\nu(Z_\nu), \tag{9}$$

where $r_{\nu\bar{\nu}}$ and $t_{\nu\bar{\nu}}$ determine the reflection and transmission coefficients normalized beforehand by group velocities (slopes of the dispersion curves) of the plane wave. Explicitly, for waves incoming in mode $\bar{\nu}$, the reflection coefficient is

$$r_{\nu\bar{\nu}} = \frac{Vg_\nu}{Vg_{\bar{\nu}}}|\xi_{\nu\bar{\nu}}|^2, \tag{10}$$

and the transmission coefficient is

$$t_{\nu\bar{\nu}} = \frac{Vg_\nu}{Vg_{\bar{\nu}}}|\eta_{\nu\bar{\nu}}|^2. \tag{11}$$

Here, $\xi_{\nu\bar{\nu}}$ and $\eta_{\nu\bar{\nu}}$ are the reflection and transmission probabilities. $Vg_{\bar{\nu}}$ is the group velocity of the incidental mode $\bar{\nu}$ and $Vg_\nu$ is that of the output channel $\nu$. As long as only one mode is excited, the problem of normalization of these coefficients by group velocities does not arise. Indeed, the sum of the reflection and transmission coefficients gives unity directly, because the momentum of the incidental mode is entirely transferred to the single outgoing mode, from where $Vg_\nu = Vg_{\bar{\nu}}$. Let us note that the velocity is set equal to zero for the evanescent modes. From their nature, these modes cannot transport energy.

With the above definitions, we only need to solve equation (1) for the masses inside the perturbed region M (irreducible set of atoms) and in the boundary columns $(-1)$ and $(n+1)$, which are matched to the rest of the perfect waveguide by equations (8) and (9). By isolating the inhomogeneous terms describing the incidental wave, we obtain an inhomogeneous system of linear equations:

$$[D_f(\Omega, \phi_y, r_3, \lambda, Z)][R]\vec{X} = -[D_f(\Omega, \phi_y, r_3, Z)]\vec{V}_{\text{in}}. \tag{12}$$

where $D_f(\Omega, \phi_y, r_3, \lambda, Z)$ indicates the defect dynamical matrix, $\vec{V}_{\text{in}}$ the incidental vector, $R$ the matching matrix and $\vec{X}$ the vector gathering all the unknown components of the

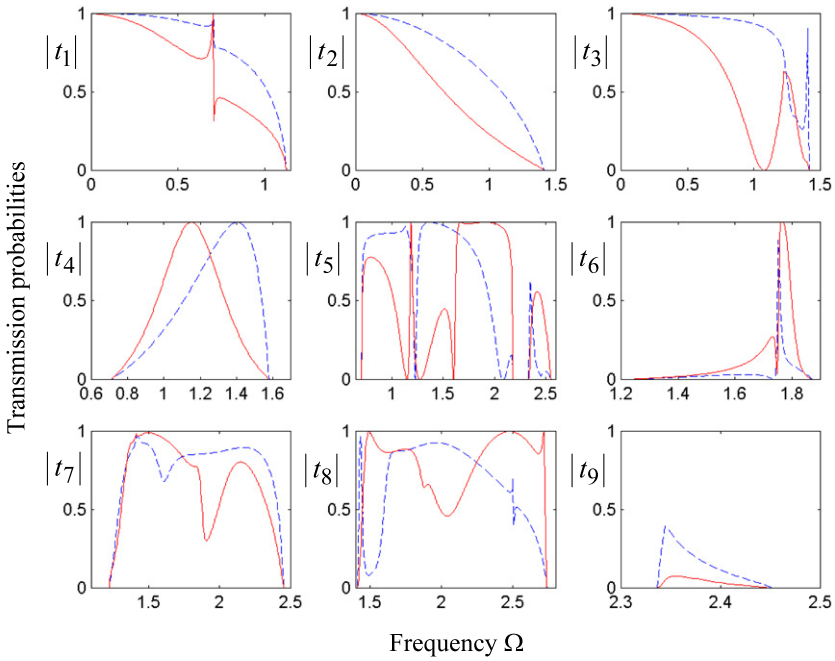


**Figure 5.** Transmission probabilities in terms of the incident phonon frequency for an isolated defect. The broken line indicates a light defect ($m' = 0.5m$) whereas the continuous line refers to the heavy defect ($m' = 2m$).

problem. For three degrees of freedom per atomic site, in the case of two defects separated by a distance $\delta = a$, the system yields 57 unknowns, namely the 39 displacement amplitudes of the perturbed region M and the nine transmission and nine reflection coefficients.

The overall transmission (or conductance) of mesoscopic disordered multichannel systems at a given frequency $\Omega$ is significant for calculating experimentally measurable physical quantities. It is then useful to define the total transmission $\Lambda$ by summing over all input and output channels:

$$\Lambda(\Omega) = \sum_{\nu} \sum_{\bar{\nu}} t_{\nu\bar{\nu}}, \tag{13}$$

where the sum is carried out over all propagating modes at the same frequency $\Omega$.

## 3. Results and discussions

The phonon scattered by a defect is analysed relative to an incidental wave coming from the left to the right (figure 1), with unit amplitude and a null dephasing on the boundary column ($-1$) of the atoms. We present the case where the elastic wave propagates parallel to the $x$ axis in the positive direction, i.e. under a null incidence angle. Calculation is carried out for lattice parameters $r_3 = 0.5$ and $\lambda = 1.2$.

### *3.1. Isolated defects*

The simplest configuration of defects to study corresponds to a linear chain of masses $m' \neq m$ arranged perpendicularly to the direction of propagation. The numerical results for the transmission probabilities in terms of the incident phonon frequency $\Omega$ are assigned in figure 5, in each mode characterizing the triple plane for two masses of defect $m' = 0.5m$ (light) and $m' = 2m$ (heavy). Conservation of energy can be used to show that $|t_\nu| + |r_\nu| = 1$, so $r_\nu$ follows immediately. This well-known theoretical relation is fortunately satisfied and always checked for each frequency. Besides, this condition constitutes an effective control method of the results.

The presence of the defect leads to a general decrease of the transmission probability. The wave is quasi-completely transmitted at low frequencies and the reflection probability then increases gradually. As expected, the influence of the defect is relatively small in the acoustic regime (modes 1, 2 and 3). However, for the heavy defect, the amplitude of the transmission spectrum decreases considerably with the mass $m'$. For $\Omega \to 0$ (centre of the Brillouin zone) we get $t_\nu \to 1$ independently of the perturbation. This generalized behaviour is also observed when backscattering becomes more significant for wavevectors near the ending zone boundary where the transmission probabilities $t_\nu$ tend towards zero, independently of the defect mass. In contrast, for optical modes 4–9, the studied transmission coefficients $t_\nu$ are null even at the first zone boundaries (points $a$, $b$, $f$ and $g$ in figure 3) because the attenuation factor modulus, at these frequencies, is less than unity (see figure 4); the corresponding modes are evanescent and the phonons located at these points do not have enough energy to follow the propagating optical branches.

As in the electronic case, strong resonance features are superposed on the monotonic transmission coefficients (figure 5). These asymmetric resonances, identified as typical Fano-like resonances, can be attributed to the presence of defect-induced resonant states, whose frequency depends on the value of the defect mass or on the relative hardening of the bonding force constant $\lambda$ in the perturbed region II. This asymmetric behaviour in the transmission spectra of

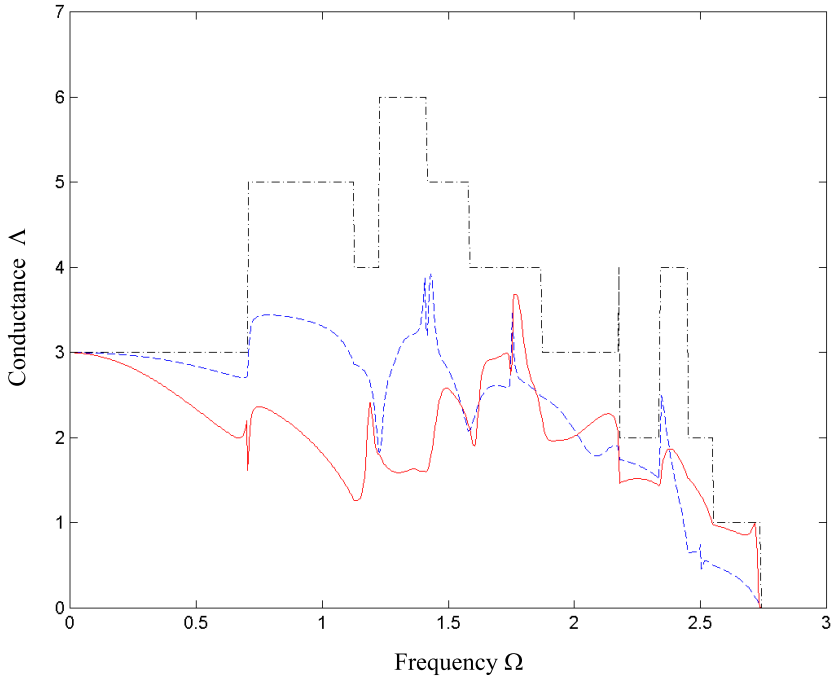


**Figure 6.** Total transmission probability for the isolated defect in the case of a null incidence. The indent-point histograms represent the total hypothetical phonon transmission capacity of the perfect waveguide consisting of three atomic infinite planes. The broken and full lines refer, respectively, to a light ($m' = 0.5m$) and a heavy defect ($m' = 2m$).

elastic waves has also been analysed in relation to phononic crystals [13].

It should be noted that the light defect also generates Anderson localized states already investigated in random layered phononic structures by Sainidou *et al* [14]. But these would be positioned at higher frequencies than those of the respective propagating modes of the local defect. Thus they cannot cause resonances in the frequency range represented in the $t_2$ spectrum, for example. A simple argument in favour of this explanation can be recalled concerning the insulated harmonic oscillator; its oscillatory frequency given by $\omega = k/m$ stipulates that a weak mass corresponds to a high vibration frequency. From the above arguments, we conclude that the resonances shift to higher (lower) frequencies for smaller (larger) defect masses. These findings are in agreement with those of Tekman and Bagwell [5], who used a two-mode approximation.

The results referring to the overall transmission $\Lambda$ of the system as a function of the dimensionless frequency $\Omega$ are shown in figure 6. In addition to the conductance spectra related to light and heavy defect masses, we also represented the ideal conductance of the perfect network (histogram in indent-point lines). In the case of the perfect network, i.e. without mass defect or force constants, we further note that the transmission probability is total in each mode. The conductance of the system then becomes significant in the frequency range where the modes overlap. For this reason it reaches a value of 6 units in the interval of propagation ranging between $\Omega \cong 1.23$ and $\Omega \cong 1.41$ (see also figure 2). The conductance spectrum is much more affected in the case of a heavy defect (full line). This influence is translated, in addition to resonance number, by a smaller amplitude compared to the light mass defect (dotted line).

In figures 7(a) and (b), we present the total transmission probabilities $\Lambda(\Omega)$ for incoming waves with oblique incidence, namely $\phi_y = \pi/4, \pi/3$. The indent-point histograms represent the total hypothetical phonon transmission capacity, with the dotted and continuous curves showing the conductance for light and heavy defects. As specified above, the frequency range of the propagating mode decreases with increasing incidence angle. The resonances due to interference between a propagating transmitted mode and a local defect mode in the perturbed region may be observed as illustrated in the previous figures. Note that these resonances shift to higher frequencies with increasing incident angle and are pronounced for oblique incidence.

### *3.2. Defect pairs*

We consider now the case of two isolated defects separated by a portion of a perfect waveguide and located at positions $l$ and $r$. The distance between the defects $\delta = (l - r)a$ is always a multiple of the network parameter. For simplicity, numerical calculations present the results for two identical defects of light mass ($m' = 0.5m$) and heavy ones ($m' = 2m$) when $r_3 = 0.5$ and $\lambda = 1.1$. The curves in figure 8 show the magnitude of the transmission coefficients for different distances in acoustic mode 2. At low frequencies, one can find that $|t_v|$ approaches unity as $\Omega \to 0$ and is independent of the lateral length $\delta$ of region II. This is because, at $\Omega \to 0$, the wavelength of the phonon is much larger than the dimension of the lateral length of the defect region and the displacement field then becomes essentially the same throughout. In this

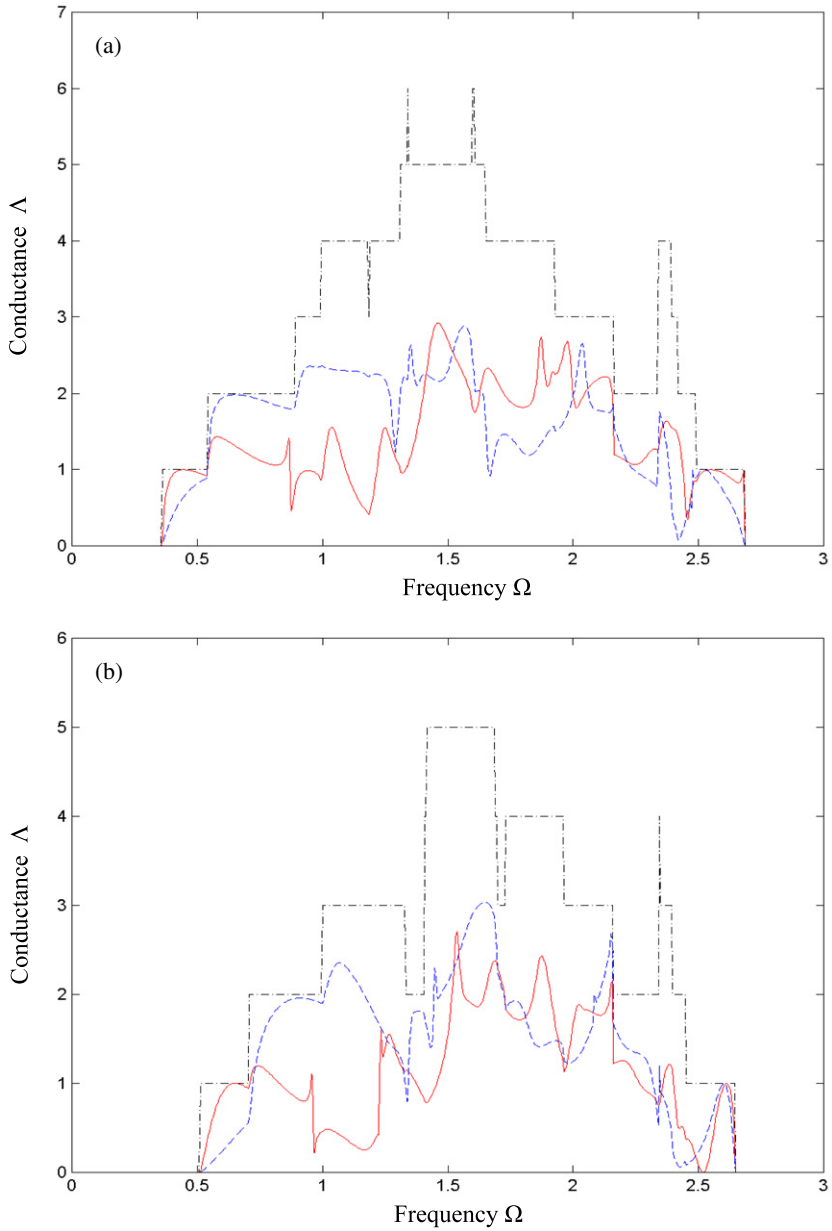


**Figure 7.** (a) The same as in figure 6 for the case of an incidence angle $\phi_y = \pi/4$. (b) The same as in figure 6 for the case of an incidence angle $\phi_y = \pi/3$.

case, the perturbed waveguide reverts to being a uniform waveguide and the phonon transmission coefficient is unity. This phenomenon, which is typical of problems in which a wave propagates through a homogeneous medium containing a finite section of a different homogeneous material, is discussed in [21] for a related problem.

It can be seen that the number of Fabry–Pérot oscillations in a given frequency interval increases as the gap widens [13]. This number depends closely on the full width $\delta$ of the defect region, which is always a multiple of the network parameter $a$. Pouthier *et al* [10] have noticed the same observations on the transmittance spectrum of a nanowire containing a set of linear clusters separated by different spacings. Our results show clearly that the two separated scatterers have all the characteristics of a Fabry–Pérot resonator. The amplitude of the oscillations is, in addition, more significant in the case of the heavy defect. Furthermore, one can find more resonance-like features occurring in the transmission spectrum with increasing incident frequency or the lateral length $\delta$ and naturally the influence of defect mass and bonding constants. Consequently, the rapid oscillations observed in the frequency range $1.2 < \Omega < 1.6$ are due to the resonances caused by the defect-induced resonant states in this region.

### *3.3. Defect distributions*

The increase in the number of defect columns $N$ results in a more important size of the linear system (10), but the matrix $D_f$ keeps its structure. The analysis becomes more and more complex. Thus we have limited our calculations to $N = 6$

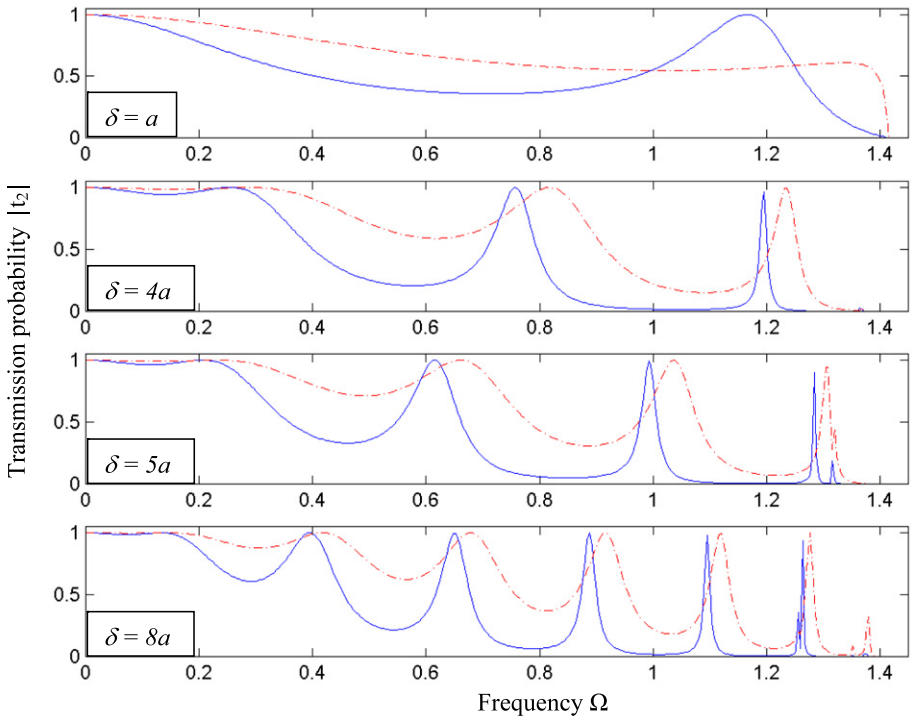


**Figure 8.** Magnitude of transmission probability in acoustic channel versus scattering frequency for two identical defects separated by a distance $\delta$. The results are given for a light defect mass ($m' = 0.5m$) by an indent-point line and for a heavy one ($m' = 2m$) by a continuous line.

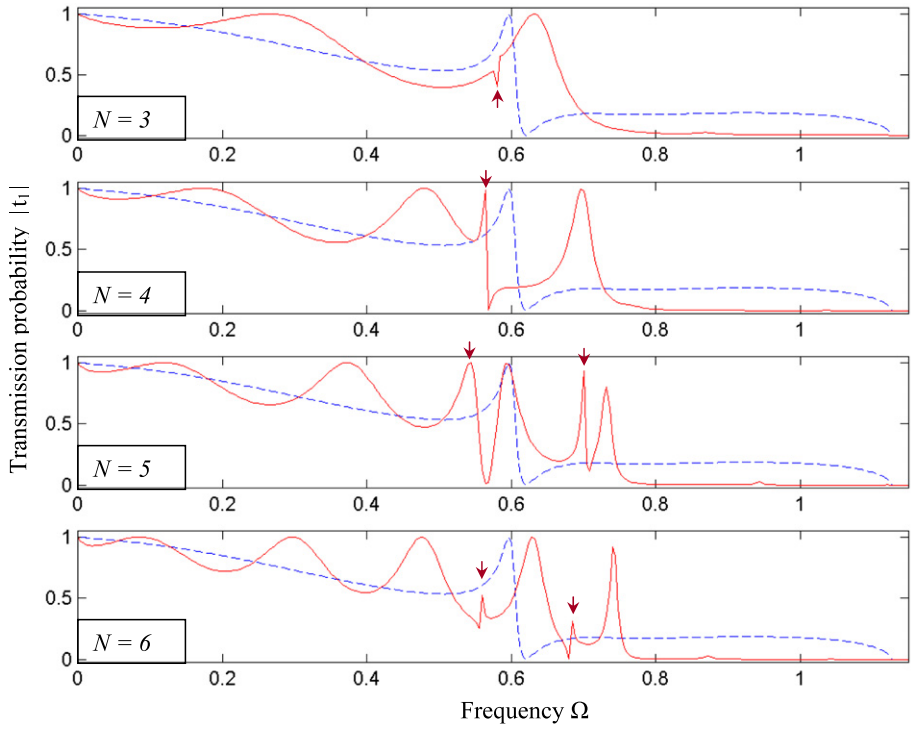


**Figure 9.** Magnitude of transmission probability in the first acoustic channel versus scattering frequency for an extended defect containing $N$ scatterers of mass $m' = 5m$. The dotted line refers to a single scatterer having the same mass. The arrows indicate the Fano-like resonance peaks.

which generates already a (117 × 135) matrix dimension. Figure 9 show the transmission coefficient in the first acoustic mode for different values of the sample thickness $N$ in the case of heavy defect $m' = 5m$. For the same reasons as those mentioned for the two preceding distributions of defects, the transmission coefficient approaches unity as $\Omega \to 0$ and is independent of the number $N$ of scatterers contained in region II. The transmission probability $|t_1|$ then decreases gradually to

the detriment of the reflection coefficient by always respecting the complementarity between the two curves as is required from the unitarity condition. Moreover, the number of Fabry–Pérot oscillations due to the interference between multiply scattered waves merges exactly with the number $N$ of defects independent of their spatial distributions. Similar results were obtained in the study of the adatomic sequences of defects separated by different spacings in a double quantum chain (quasi-1D waveguide) [22]. Also, these observations indicate that this defect provision behaves like a Fabry–Pérot resonator. As in the case of a single defect (dotted curve in figure 9), the transmission spectrum for $N \leqslant 3$ presents only one Fano-like resonance. The resonance frequency decreases slightly with $N$. Quite surprisingly, from $N \geqslant 4$, we obtain a second resonance structure in the upper frequency range which is apparently due to a second resonant state in this region. For large $N$, the separation between the localized states becomes very small. Moreover, the resonance minima do not necessarily reach zero value, as is usually the case for defects which are extended in the direction of propagation.

Owing to the fact that the resistance opposed to the passage of the wave in the perturbed area becomes more significant for the heavy mass defect, the amplitude in transmission spectra is more affected than that referring to the light mass. This influence also results in a higher resonance number because of certain localized states, suitable for the light defect, are localized at frequencies higher than those of the implied propagating mode frequencies, as underlined previously in the case of an isolated defect. This phenomenon was also observed in [16] while varying $\lambda$. Thus, the variation of the mass plays the same role as that of the $\lambda$ parameter. As may be expected, we find that defects lead always to an increase of resistance, irrespective of their local distribution.

## 4. Conclusion

In this work, we have recourse to the matching method to treat the scattering of vibrational waves by multichannel quasi-three-dimensional disordered mesoscopic systems while solving the Newton dynamical equation within the harmonic approximation framework. The undulatory behaviour of the wave through a defect was analysed by taking account of defect mass variation and the bonding strengths in the perturbed region. We have investigated phonon transmission and conductance for three bulk defect configurations (isolated, separated and extended defects) considering different incidences. The presence of a defect in a crystalline nanostructure modifies particularly its mechanical properties by the creation of new localized states and by bulk phonon scattering [9] and also surface phonon scattering [11, 22]. Its influence results in a generalized decrease of the transmission spectrum amplitude accentuated by Fabry–Pérot oscillations (due to the interference between multiply reflected waves in region II) and Fano-like resonances (coupling between propagating transmitted modes and local defect-induced modes that are embedded in the continuum). It is observed that this type of resonance shifts to higher (lower) frequencies for smaller (larger) defect masses following the well-known relation $\omega = \sqrt{k/m}$. In contrast, the number of Fabry–Pérot oscillations in a given frequency depends closely on the full width of the defect region. The amplitude of the oscillations is, in addition, more pronounced in the case of the heavy defect. As expected, the influence of the light defect is smaller than the heavy defect. The transmission or conductance spectra can thus be regarded as fingerprints of the specific defect structure and therefore be used for the characterization.

The interaction between defect-induced states and propagating waveguide eigenmodes could provide an interesting alternative to investigate structural properties. Although measurements of transmission probabilities are rather difficult, direct measurements of total transmission $\Lambda(\Omega)$ should be feasible. The experimental challenge would consist in coupling a receiver and a transmitter with known frequency characteristics at the ends of the waveguide by avoiding the possible back reflections at the junctions. The interference effects are of interest for improvements in the design of transducers and noise control [23, 24] whereas Fano-type resonances are commonly used to build filters [25].

It should be noted that the interference phenomena discussed in this paper are derived from the dynamical equations in the harmonic approximation which can be applied to any length scale, provided that the phase coherence is not destroyed by dissipative effects. In other words, the model can equally influence the interference effects induced in the macroscopic systems, and it is hence possible to test the theoretical results via an experiment using laboratory scale masses (balls), binding springs and wave generators, as in acoustic studies.

## References


[1] Kramer B 1991 *Quantum Coherence in Mesoscopic Systems* (New York: Plenum)
[2] Ibach H and Mills D L 1982 *Electron Energy Loss Spectroscopy and Surface Vibrations* (New York: Academic)
[3] Landauer R 1987 *Z. Phys.* B **68** 217
Landauer R 1989 *J. Phys.: Condens. Matter* **1** 8099
[4] Khater A, Auby N and Kechrakos D 1992 *J. Phys.: Condens. Matter* **4** 3743
[5] Tekman E and Bagwell P F 1994 *Phys. Rev.* B **48** 18299
[6] Gagel F and Maschke K 1995 *Phys. Rev.* B **52** 2013
[7] Berthod C, Gagel F and Maschke K 1994 *Phys. Rev.* B **50** 18299
[8] Virlouvet A, Grimech H, Khater A, Pennec Y and Maschke K 1996 *J. Phys.: Condens. Matter* **8** 7589
[9] Fellay A, Gagel F, Maschke K, Virlouvet A and Khater A 1997 *Phys. Rev.* B **55** 1707
[10] Pouthier V and Girardet C 2002 *Phys. Rev.* B **66** 115322
[11] Rabia M S, Aouchiche H and Lamrous O 2003 *Eur. Phys. J.—A.P.* **23** 95–102
[12] Maradudin A A, Montroll E W, Weiss G H and Patova I 1971 *Theory of Lattice Dynamics in the Harmonic Approximation* (New York: Academic)
[13] Sainidou R and Stefanou N 2006 *Phys. Rev.* B **73** 184301
[14] Sainidou R, Stefanou N and Modinos A 2005 *Phys. Rev. Lett.* **94** 205503
[15] Feuchtwang T E 1967 *Phys. Rev.* **155** 731
[16] Szeftel J and Khater A 1987 *J. Phys. C: Solid State Phys.* **20** 4725
[17] Van Hoove L 1953 *Phys. Rev.* **89** 1189

[18] Landau I and Lifshitz E 1967 *Théorie de l'Elasticité* (Moscow: Mir) p 146
[19] Marcuse D 1991 *Quantum Electronics—Principles and Applications* ed P F Liao and P L Kelley (New York: Academic)
[20] Sainidou R, Stefanou N, Psarobas I E and Modinos A 2005 *Comput. Phys. Commun.* **166** 197
[21] Meylan M H and Squire V A 1993 Finite-flow wave reflection and transmission coefficients from a semi-infinite model *J. Geophys. Res.* **98** 537–42
[22] Rabia M S 2006 Surface defects characterization in quantum wires by acoustical phonons scattering *J. Mol. Struct.-Theochem.* **777** 131–8
[23] Guglielmi M, Montauti F, Pellegrini L and Arcioni P 1995 *IEEE Trans. Microw. Theory Tech.* **43** 1991
[24] Wolfe J P 1995 *Phys. Today* **70** 34
[25] Kushwaha M S, Akjouj A, Djafari-Rouhani B, Dobrzynski L and Vasseur J O 1998 *Solid State Commun.* **106** 659